JBC RESEARCH ARTICLE

Characterization of a nitrite-reducing octaheme hydroxylamine oxidoreductase that lacks the tyrosine cross-link

Received for publication, January 29, 2021, and in revised form, February 18, 2021 Published, Papers in Press, February 27, 2021,
https://doi.org/10.1016/j.jbc.2021.100476

Christina Ferousi[1], **Rob A. Schmitz**[1], **Wouter J. Maalcke**[1], **Simon Lindhoud**[1], **Wouter Versantvoort**[1], **Mike S. M. Jetten**[1], **Joachim Reimann**[1], **and Boran Kartal**[2,*]

From the [1]*Department of Microbiology, Institute for Water and Wetland Research, Radboud University, Nijmegen, The Netherlands;* [2]*Microbial Physiology Group, Max Planck Institute for Marine Microbiology, Bremen, Germany*

Edited by Ruma Banerjee

The hydroxylamine oxidoreductase (HAO) family consists of octaheme proteins that harbor seven bis-His ligated electron-transferring hemes and one 5-coordinate catalytic heme with His axial ligation. Oxidative HAOs have a homotrimeric configuration with the monomers covalently attached to each other *via* a unique double cross-link between a Tyr residue and the catalytic heme moiety of an adjacent subunit. This cross-linked active site heme, termed the P460 cofactor, has been hypothesized to modulate enzyme reactivity toward oxidative catalysis. Conversely, the absence of this cross-link is predicted to favor reductive catalysis. However, this prediction has not been directly tested. In this study, an HAO homolog that lacks the heme-Tyr cross-link (HAOr) was purified to homogeneity from the nitrite-dependent anaerobic ammonium-oxidizing (anammox) bacterium *Kuenenia stuttgartiensis*, and its catalytic and spectroscopic properties were assessed. We show that HAOr reduced nitrite to nitric oxide and also reduced nitric oxide and hydroxylamine as nonphysiological substrates. In contrast, HAOr was not able to oxidize hydroxylamine or hydrazine supporting the notion that cross-link-deficient HAO enzymes are reductases. Compared with oxidative HAOs, we found that HAOr harbors an active site heme with a higher (at least 80 mV) midpoint potential and a much lower degree of porphyrin ruffling. Based on the physiology of anammox bacteria and our results, we propose that HAOr reduces nitrite to nitric oxide *in vivo*, providing anammox bacteria with NO, which they use to activate ammonium in the absence of oxygen.

Cytochrome *c* proteins are among the most common redox tools in nature and are ubiquitous in all domains of life (1). The electron configuration of elemental iron in combination with both the electrochemical properties of the heme porphyrin and the structural and functional contributions from the protein backbone renders heme *c* cofactors suitable for catalysis and electron transfer. This versatility is further enhanced by the arrangement of two or more heme cofactors within a protein as seen in the multiheme cytochromes *c* (MCCs). This class of proteins is involved in prokaryotic energy metabolism ranging from intra- or extracellular electron transfer to substrate conversion (2–5). Within the MCCs, the hydroxylamine oxidoreductase (HAO) protein family constitutes the largest group of octaheme cytochromes *c* (OCCs) next to the octaheme nitrite and tetrathionate reductases (ONRs and OTRs, respectively) (6–10).

The HAO family comprises enzymes that harbor eight $CX_{2-4}CH$ heme-binding motifs, but otherwise exhibits low primary structure similarity (10, 11). HAOs harbor seven bis-His ligated electron-transferring hemes and one 5-coordinate catalytic heme with a His axial ligation (12–14). *In vitro*, isolated HAOs are catalytically versatile and can perform hydrazine (N_2H_4) and hydroxylamine (NH_2OH) oxidation, as well as nitrite (NO_2^-), nitric oxide (NO), and NH_2OH reduction, albeit at varying catalytic efficiencies (2, 15–17). Under physiological conditions, however, three of the four structurally characterized representatives perform oxidative catalysis with high catalytic efficiencies (0.1–12 s^{-1} μM^{-1}) (14, 18, 19). Both the HAO from the aerobic ammonia-oxidizing bacteria—*Nitrosomonas europaea* (NeHAO) (12, 16, 18)—and the HAO from the anaerobic ammonium-oxidizing (anammox) bacteria—*Kuenenia stuttgartiensis* (KsHAO) (14)—catalyze NH_2OH oxidation to NO, while hydrazine dehydrogenase from *K. stuttgartiensis* (KsHDH) oxidizes N_2H_4 to dinitrogen gas (N_2) and is, interestingly, inhibited by both NO and NH_2OH at low μM concentrations (19, 20).

Oxidative HAOs display high tertiary and quaternary similarity, all adopting a homotrimeric configuration (14) (or multiples thereof) (20), with the monomers covalently attached to each other *via* a unique double cross-link: The C3 and the phenolate oxygen atoms of a Tyr are attached to the C5 and C4 atoms of the catalytic heme moiety of an adjacent subunit. This cross-link results in a diagnostic Soret

* For correspondence: Boran Kartal, bkartal@mpi-bremen.de.
Present address for Christina Ferousi: Industrial Biotechnology & Biocatalysis Group, Biotechnology Laboratory, School of Chemical Engineering, National Technical University of Athens, 5 Iroon Polytechniou Str., Zografou Campus, Athens 15780, Greece.
Present address for Simon Lindhoud: Laboratory of Biochemistry, Wageningen University, Wageningen 6708 WE, The Netherlands.
Present address for Wouter J. Maalcke: Synthon BV, Microweg 22, Nijmegen 6545 CM, The Netherlands.

absorption feature of the reduced protein in the wavelength range of 463 to 475 nm (14, 19, 21), which lends the prosthetic group its name—the P460 cofactor (also see cytochrome P460) (22). The Tyr cross-link in the P460 active site of HAO has long been hypothesized to modulate enzyme reactivity toward oxidative catalysis; accordingly, its absence is predicted to favor reduction (11, 23).

Four HAO genes from εProteobacteria (εHAOs) that lack the critical Tyr residue were recombinantly expressed and shown to reduce NO_2^- and NH_2OH *in vitro* (V_{max} = 1–180 U mg protein^{-1}), while their NH_2OH-oxidizing activity was negligible (highest V_{max} = 0.07 ± 0.05 U mg protein^{-1}) (24). Additionally, the structure of an HAO—the gene product of kustc0458 from *K. stuttgartiensis*—that is predicted to be reductive based on physiological experiments (23) and proteomic analyses (25), was recently resolved (26). The structure of Kustc0458 revealed the absence of the heme-Tyr cross-link but otherwise highlighted the high structural conservation within the HAO family. Kustc0458 crystallized as a heterododecamer ($\alpha_6\beta_6$) with a diheme cytochrome *c* (Kustc0457; DH), resulting in a total of 60 hemes for the Kustc0458/7 protein complex (26). Based on the structure, the heterohexamer ($\alpha_3\beta_3$) presents the largest possible heme circuit within the complex and complies with the heme ring arrangement that is seen in all oxidative HAOs. In this case, the heme ring is modified by the addition of two 6-coordinate hemes, contributed by the DH subunits, at each HAO surface heme (heme 1). In analogy with the oxidative HAOs, the Kustc0458/7 catalytic protomer (αβ) comprises nine hemes with saturated coordination—seven HAO bis-His and two DH His/Met ligated hemes—and one 5-coordinate HAO His-ligated heme (heme 4). Kustc0458 is highly transcribed and expressed in *K. stuttgartiensis* cells under standard laboratory growth conditions (27) and has been localized within the anammoxosome (28), a bacterial organelle where the main anammox catabolism takes place (29, 30).

The anammox pathway proceeds through NO_2^- reduction to NO, subsequent comproportionation of ammonium (NH_4^+) and NO by hydrazine synthase (HZS), and the final oxidation of N_2H_4 to N_2 by HDH (**Reactions 1–3**) (19, 27, 31). The low-potential electrons released from the oxidation of N_2H_4 are used for cell carbon fixation and other cellular anabolic reactions (23).

$$NO_2^- + 2H^+ + e^- \rightarrow NO + H_2O \left(E_0' = +380\ mV\right) \quad (1)$$

$$NO + NH_4^+ + 2H^+ + 3e^- \rightarrow N_2H_4 + H_2O \left(E_0' = +60\ mV\right) \quad (2)$$

$$N_2H_4 \rightarrow N_2 + 4H^+ + 4e^- \left(E_0' = -750\ mV\right) \quad (3)$$

In the absence of nitrite, *K. stuttgartiensis* can grow on NO and NH_4^+ instead (25). During this NO-dependent anaerobic NH_4^+ oxidation, transcription of both Kustc0458 and Kustc0457 was strongly downregulated (28- and 39-fold, respectively). Additionally, the only NO-forming nitrite reductase identified in the *K. stuttgartiensis* genome (cd_1NiR homolog) had low abundance in both transcriptomes and proteomes obtained under standard and NO-dependent growth conditions (25, 27). Furthermore, neither cd_1 cytochrome (cd_1NiR) nor copper-containing (CuNiR) nitrite reductase homologs are conserved among anammox genomes, while the orthologs of Kustc0458 are present in all known anammox genera (26). Based on *in vivo* observations from *K. stuttgartiensis*, Kustc0458 was implicated in the reduction of nitrite to NO, the first step of the anammox pathway (23). In this study, we purified the native Kustc0458/7 complex from *K. stuttgartiensis* biomass, assessed its catalytic potential involving physiologically relevant nitrogen species and showed that this protein reduces nitrite to NO. Our findings are examined in the context of the HAO protein family, and the physiological relevance of Kustc0458/7 is discussed.

Results

Kustc0458 was consistently purified from *K. stuttgartiensis* single-cell enrichment cultures in an equimolar complex with Kustc0457. Native and sodium dodecyl sulfate (SDS)-denaturing polyacrylamide gel electrophoresis (PAGE) migration profiles indicated a stable, noncovalent dodecameric composition for the complex in solution that is in agreement with the crystallographically resolved structure (26). The electronic absorption spectra of the fully reduced protein revealed the absence of the characteristic P460 absorption feature (Fig. 1), in line with the absence of the Tyr cross-link. Fully oxidized (as isolated) Kustc0458/7 displayed a Soret maximum at 409 nm, which broadened and shifted to 415 nm upon partial reduction by ascorbate. Full reduction by dithionite resulted in a sharp Soret at 419.5 nm, a subtle shoulder at 425 nm, and Q band maxima at 524 and 553 nm. Notably, despite the Met axial ligation of both DH heme iron centers (26), no charge transfer band at 695 nm was observed.

Kinetic properties

To test whether the Tyr cross-link is necessary for oxidative catalysis, we probed the capacity of Kustc0458/7 to oxidize NH_2OH and N_2H_4 spectroscopically. Depending on the sample preparation, the measured rates were ranging from zero to about 0.020 U mg^{-1} for both substrates, which is 100- to 1000-fold slower compared with the anammox oxidative HAOs and NeHAO, respectively. Notably, both anammox oxidative HAOs are among the most abundant proteins in *K. stuttgartiensis* cells (27) and hence, even a minute (*i.e.*, ∼0.5%) contamination of the Kustc0458/7 sample with either KsHAO or KsHDH (for NH_2OH or N_2H_4 oxidation, respectively) could explain the measured rates, strongly suggesting that Kustc0458/7 is not an oxidative catalyst. Reductive reactivity of Kustc0458/7 toward NO_2^-, NO, and NH_2OH was investigated by monitoring the oxidation of the methyl viologen monocation radical (MVred) (32). At 50 μM substrate concentration, NO_2^- reduction proceeded at 0.1 U mg^{-1} while

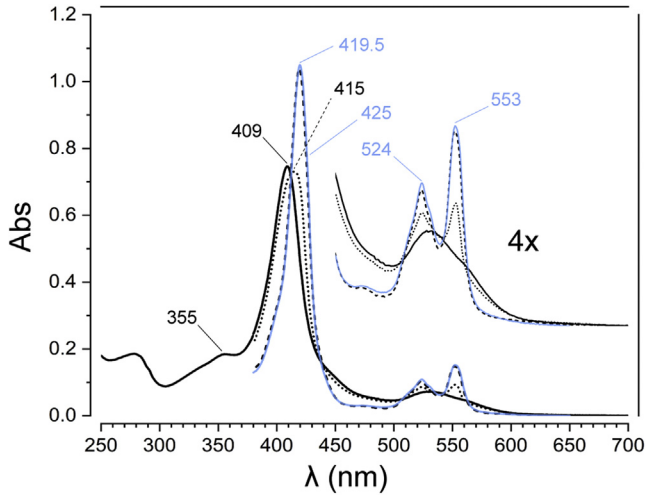

Figure 1. Electronic absorption spectra of 0.8 μM Kustc0458/7. As isolated (*fully oxidized*; *solid black line*), ascorbate reduced (*dotted black line*), and dithionite reduced (*dashed black line*). Titanium citrate addition to the isolated protein resulted in the same fully reduced spectrum (*solid blue line*) as seen with dithionite addition. The spectrum of as-isolated Kustc0458/7 for the 250 to 380 nm range is extracted from a different data set and has been corrected for heme concentration (at 409 nm). The inset shows a fourfold magnification of the 450 to 700 nm region

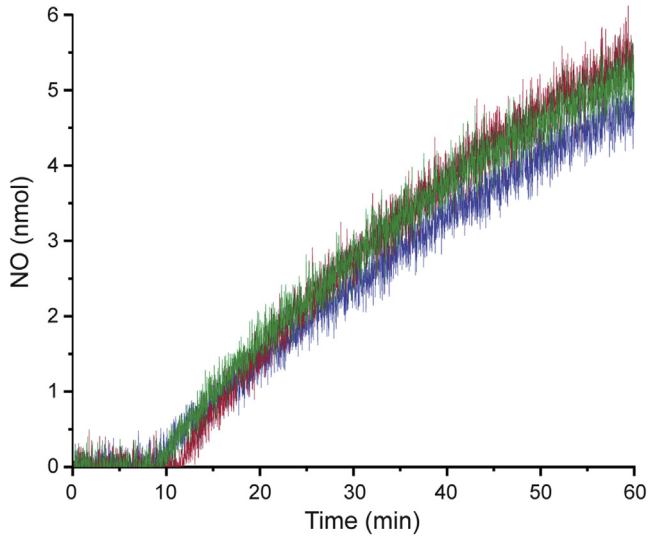

Figure 2. Reduction of nitrite to NO by HAOr. NO is produced after addition of 50 μM nitrite (at 10 min) in the presence of 200 μM phenazine ethosulfate and 100 μM ascorbate. The assay was carried out at pH 7.5 and 30 °C, and NO was measured with membrane-inlet mass spectrometry. Each *colored line* corresponds to a biological replicate

NO and NH_2OH were consistently faster (2.8 and 4.6 U mg^{-1}, respectively). Similar kinetic trends have been observed for the ammonia-producing respiratory cytochrome *c* nitrite reductase (ccNiR) and were explained by the presumed higher activation entropy for hydroxylamine reduction (33).

Colorimetric determination of ammonia after completion of each reductive assay routinely returned the same substrate-to-product ratios: 1:0.6, 1:1, and 1:1 for NO_2^-, NO, and NH_2OH, respectively. The stoichiometric nitrogen imbalance observed for nitrite conversion is presumably due to the release of at least one catalytic intermediate from the Kustc0458/7 active site during catalysis *in vitro*. Given the reducing environment in the assay achieved by excess MVred and the higher catalytic rates of Kustc0458/7 for the downstream reactions at relevant concentrations, *i.e.*, NO and NH_2OH reduction, this observation could only be attributed to finely tuned binding equilibria that could possibly be affected by redox modulations of the extended 9-heme network per active site.

In order to determine whether Kustc0458/7 performed its predicted physiological function of nitrite reduction to NO, different artificial electron carriers were used with nitrite as the substrate. The reducing environment created by excess MVred and the reactivity of NO prevented the direct measurement of NO when MVred was used as the electron carrier. To circumvent this problem, phenazine ethosulfate, which has a much higher midpoint potential (E'_0 = +55 mV) compared with MV (E'_0 = −440 mV), was used as an electron carrier to directly measure NO production in membrane-inlet mass spectrometry (MIMS) experiments. Here, when the reaction was initiated with the addition of nitrite, stable and reproducible NO production was detected at a rate of 0.52 mU mg^{-1} (Fig. 2). Colorimetric nitrite measurements at the end of these experiments showed that all nitrite reduction could be accounted for by the produced NO and no other nitrogenous species such as hydroxylamine or ammonium were produced.

Based on these results, we conclude that the Kustc0458/7 protein complex is a NO-producing reductive HAO that is incompetent for oxidative catalysis. Whereas HAOr from *K. stuttgartiensis* and HAOs from Epsilonproteobacteria all lack appreciable *in vitro* oxidative activity (24), oxidative HAO complexes, conversely, have been shown to act as reductases *in vitro*, albeit with diverse rates. Both NeHAO and KsHAO can reduce NO_2^-, and NeHAO can also reduce NO and NH_2OH, demonstrating that the HAO active site architecture is inherently competent for substrate reduction (14–16). In fact, it is the oxidation state of the heme Fe in NeHAO that presumably dictates the redox direction toward hydroxylamine as well as the observed rates. By comparing hydroxylamine reductase activity among NeHAO, myoglobin, and catalase, Kostera *et al.* (16) showed that a reduced active site led to conversion rates 100-fold greater than those observed for the ferric enzyme, concluding that the redox equilibrium during catalysis heavily determines the reactivity of the enzyme.

Effects of substrate additions

Nitrite titration (1 μM–2.2 mM) of reduced HAOr (Fig. 3*A*) first resulted in the oxidation of the residual dithionite—most likely by nonenzymatic reduction of NO_2^- to NO. Subsequently, a feature peaking at 354 nm, probably indicative of nitrite (π→π* transition) (34), grew in. Notably, free NO gas also features a transition in the same wavelength range and so does the heme porphyrin (35) as exemplified in the spectrum of fully oxidized HAOr (N band maximum at 355 nm; Fig. 1). This overlap of multiple absorbing species restricts any direct conclusions, but the presence of free NO in the cuvette, released from a putative iron-nitrosyl intermediate during partial nitrite turnover, remains possible.

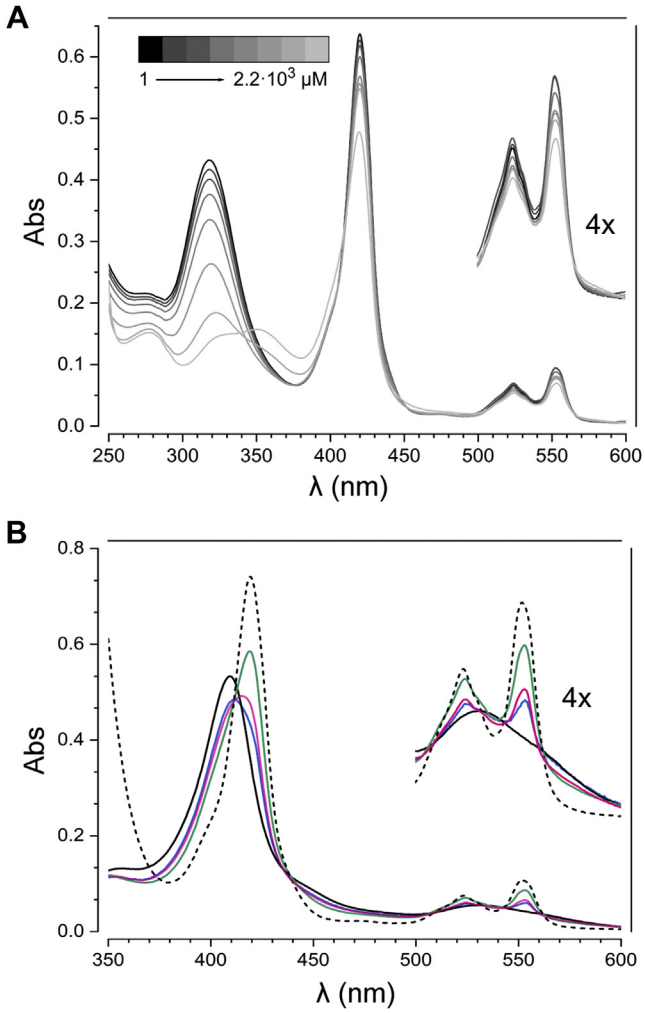

Figure 3. Titration of Kustc0458/7 with different substrates. *A*, nitrite titration of fully reduced Kustc0458/7 (1.5 µM active sites). *Black* to *gray*: 1 µM, 2 µM, 3 µM, 13 µM, 113 µM, 213 µM, 1.2 mM, and 2.2 mM. The *inset* shows a fourfold magnification of the 500 to 600 nm region. The Soret signal decrease is due to dilution. The peak at 314 nm corresponds to dithionite. Excess of reductant was necessary to keep Kustc0458/7 in the fully reduced state, which would get partially oxidized otherwise, even under strictly anaerobic conditions. *B*, electronic absorption spectra of 0.6 µM Kustc0458/7, (*fully oxidized*; *solid black line*), after addition of 2 mM hydrazine to the fully oxidized enzyme (*green*), after addition of 2 mM hydroxylamine to the fully oxidized enzyme (*blue*), after addition of 10 mM hydroxylamine to the fully reduced enzyme (*pink*), and fully reduced enzyme (*dashed black line*).

When fully oxidized HAOr was incubated with excess NH_2OH, the protein became partially reduced with a new red-shifted Soret maximum, distinct Q bands, and a narrow shoulder around 420 nm (Blue line, Fig. 3*B*). Interestingly, addition of excess NH_2OH to fully reduced HAOr resulted in a similar spectrum with a more pronounced 420 feature (Pink line, Fig. 3*B*), which could be indicative of a Fe^{II}-NH_2OH adduct.

Potentiometric redox titration

The sheer heme count in each HAOr catalytic protomer (αβ) along with the absence of any spectroscopic handle for the active site heme 4 poses limitations to the direct determination of the midpoint potentials of individual heme centers. To better inform our hypotheses, however, we performed electrochemical redox titrations of HAOr coupled to UV/Vis spectroscopy. The complete redox transition of HAOr occurred in a range over 600 mV *versus* the standard hydrogen electrode (*versus* SHE; this reference is used throughout the paper) and Nernst global fittings of the spectra discerned five redox transitions: Em_1 = +305 mV; Em_2 = +92 mV; Em_3 = −41 mV; Em_4 = −175 mV; Em_5 = −315 mV (Fig. 4*A*). The first two transitions (Em_1 and Em_2) exhibited Soret maxima at 422 and 420 nm, respectively, and their corresponding α bands were centered around 554 nm (Fig. 4*B*). In the spectrum corresponding to the third transition (Em_3 = −41 mV), the Soret peaked at 422 nm and the α band was split with maxima at 552 and 556 nm, respectively. The fourth transition (Em_4 = −175 mV) featured a wide and red-shifted Soret peaking at 420 and 425 nm, while the spectrum of the last redox transition (Em_5 = −315 mV) presented two Soret maxima at 421 and 426 nm, respectively, as well as a split α band peaking at 552 and 557 nm. The red-shifted Soret maxima of the latter two transitions imply the growth of a low-energy Soret species that is usually indicative of high-spin Fe^{II} heme centers (36) and could therefore correspond to the HAOr active site heme. However, the relative intensities at longer wavelengths imply complete reduction of this high-spin species already at potentials higher than −175 mV.

Since not all five transitions contributed equally to the total redox change of the system, we used difference spectra corresponding to each redox transition to unravel the number of hemes contributing to each transition. We assumed a total contribution of ten redox centers for the Soret and nine for the α band, excluding the structurally resolved HAOr heme 4 that has a His/H_2O iron coordination and is expected to have low extinctions at the Q region of the spectrum. The sum of the differences between the heme count from the Soret area and the α band, respectively, corresponds to the single unaccounted heme, *i.e.*, the catalytic heme. Based on this approach, transitions 1, 3, and 4 collectively accounted for the bulk of this difference, corroborating the higher redox potential of HAOr heme 4 compared with its oxidative counterparts that range between −260 and −420 mV (Fig. 4*C*) (14, 19, 37).

Based on the NeHAO kinetic studies discussed above (16), oxidative HAOs essentially require reduced active sites for efficient NH_2OH reduction, which is a nonphysiological reactivity for all biochemically characterized homologs (14, 16, 17, 19). Harboring a catalytic heme with a low redox potential substantially increases the possibility of the heme Fe always being oxidized under physiological conditions and, thus, favoring oxidative catalysis. To the contrary, reductive HAOs, represented by HAOr, are catalytically competent only for substrate reduction, which requires reductive conditions. They, therefore, feature a higher redox potential catalytic heme that can afford physiological catalysis without any side reactions.

Low reduction potentials of heme cofactors have been associated with increased heme ruffling (38–40), a structural out-of-plane (OOP) distortion of the porphyrin that results in the absence of any overlap between the Fe d-orbitals manifold

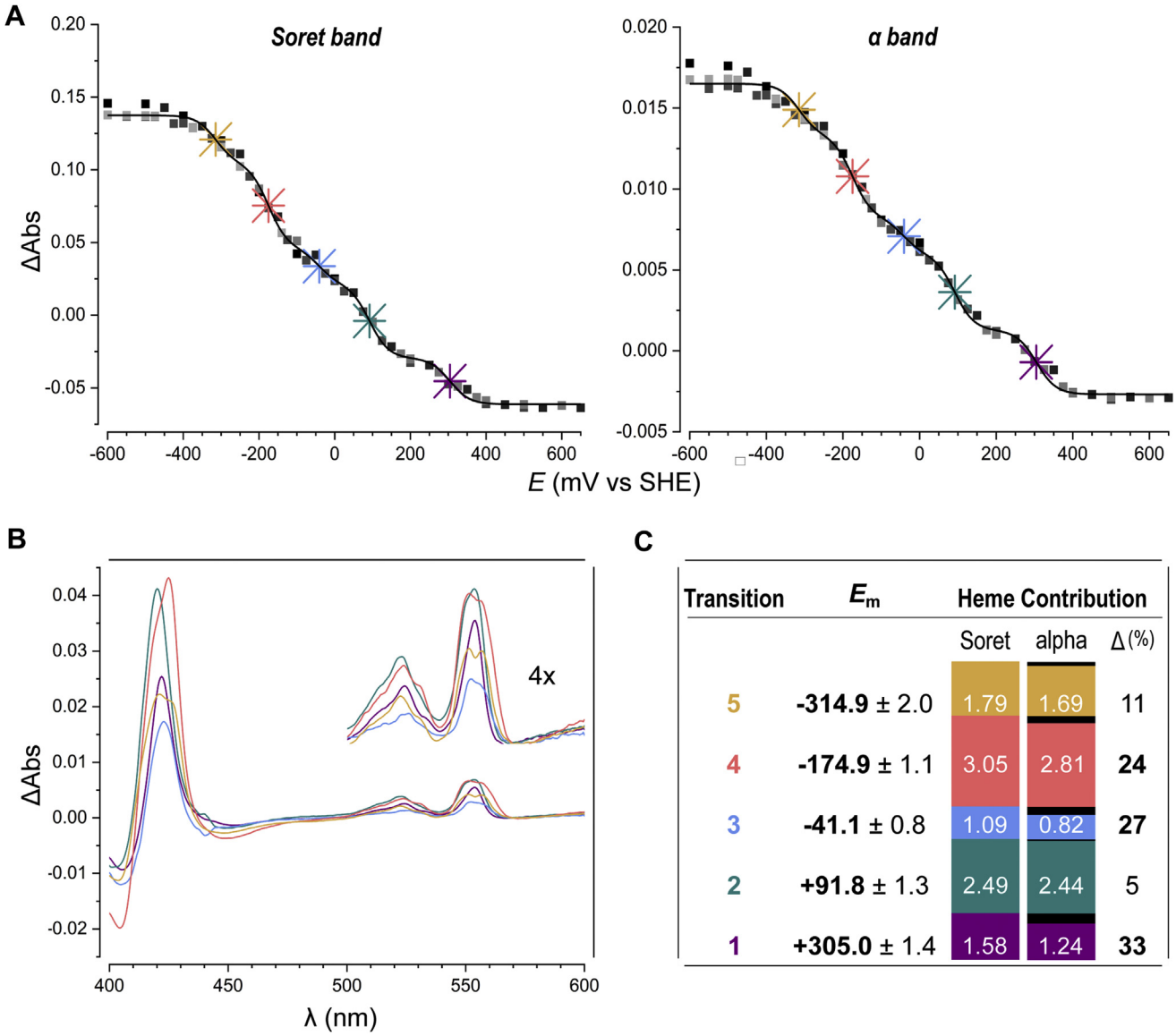

Figure 4. Potentiometric redox titration of 50 μM Kustc0458/7 performed in both reductive and oxidative directions. Global spectra Nernst fitting discerned five redox transitions; the midpoint potentials of each (with one standard deviation) and the color code used for the transitions are shown in panel *C*. *A*, ΔAbsorbance values corresponding to the Soret (420–404 nm) and the α band (552–544 nm) are independently plotted against the applied potentials and fitted to a Nernst equation with five components and fixed potentials—as discerned by the global spectra fits. Grayscale indicates different data series in either oxidizing or reductive direction during the titration, illustrating the stability of the electrochemical system throughout the experiment. Nernst fittings are shown in black lines and the points corresponding to the discerned *Em* values are shown as crosses. *B*, difference spectra corresponding to each of the five redox transitions. *C*, the mathematical areas corresponding to the Soret and the α bands (411–434 nm and 540–570 nm, respectively) were calculated for all discerned transitions and for the total. Assuming contribution of ten hemes to the total Soret area change and nine to the alpha band, the number of hemes contributing to each redox transition was calculated, based on both the Soret and the α band changes (*color-coded bars* and numbers therein). The difference between the heme count from the Soret and the α band (Δ% bar) corresponds to a fraction of one unaccounted heme, *i.e.*, the catalytic heme.

and the porphyrin π system of the heme (41). Subjecting all four structurally resolved HAO homologs in a quantitative analysis assessing different heme distortions (42, 43) underlined another difference between HAOr and the three oxidative HAOs (Fig. 5 and Table S1). The HAOr catalytic heme exhibits a lower overall OOP distortion, with the most substantial difference in the degree of ruffling that is about 50% lower compared with oxidative HAOs.

Heme ruffling enforces an electronic ground state of iron that results in lower reduction potentials (41, 44, 45) and appears to promote the stability of $\{FeNO\}^6$ adducts against reductive nitrosylation, which could lead to stable off-pathway intermediates (22, 44–46). Interestingly, while the dissociation of NO from fully reduced *b*- and *c*-type heme nitrosyls is usually very slow (10^{-3}–10^{-5} s^{-1}), cd_1NiR releases NO from its unique Fe^{II} d_1 active site about 1000-fold faster (47), presumably due to an orchestrated and dynamic hydrogen-bonding network established by the protein scaffold (48). NO dissociation from the putative iron-nitrosyl intermediate of HAOr that was formed during nitrite reduction *in vitro*

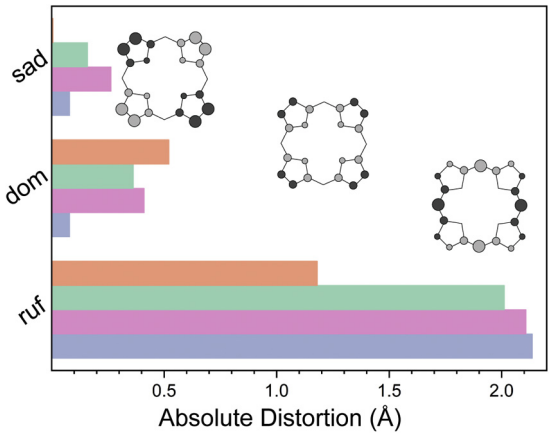

Figure 5. Out-of-plane (OOP) heme displacements. (Sad: saddling; dom: doming; ruf: ruffling) were calculated for NeHAO (*blue*), KsHAO (*pink*), KsHDH (*green*), and Kustc0458/7 (*orange*). The *inset* shows a schematic representation of the heme porphyrin with each OOP distortion, where the *dark circles* represent atomic positions above and the *light circles* below the heme plane. The *inset* is adapted with permission from Jentzen *et al.* (43). Copyright 1997 American Chemical Society. The complete output can be found in the Table S1.

could account for the measured discrepancy in the nitrogen balance during ammonia determination (60% N-NH_3). Under the heavily reducing conditions of the *in vitro* assay (MVred excess), it is conceivable that the HAOr active site is in a super-reduced state. Upon one-electron reduction of nitrite to NO, the latter dissociates from a reduced heme at rates comparable to the rate of overall electron consumption. If this holds true under physiological conditions, HAOr presents another exception of on-pathway $\{FeNO\}^7$ intermediates, next to cd_1NiR.

Discussion

Pentaheme ccNiR, OTR, and ONR can all reduce nitrite, albeit with different catalytic efficiencies, and share similar active site architectures, with the most remarkable being the Lys proximal ligand of the heme Fe (6, 9, 49). Interestingly ccNiR and ONR code for this Fe-ligating Lys within a conserved CXXCK heme-binding sequence, while OTR harbors the typical CXXCH motif instead. Both ccNiR and ONR feature a catalytic triad composed of tyrosine, histidine, and arginine at the distal side of their catalytic heme that appears to tune the proton-coupled redox steps during nitrite turnover (50, 51). A point mutation of this Tyr in the ccNiR from *Wolinella succinogenes* resulted in an over 90% decrease of the produced ammonia during nitrite reduction *in vitro*, while the conversion rates appeared unaffected (52). One-electron reduction of nitrite and subsequent release of NO from the mutated ccNiR active site could offer a plausible explanation for these observations and further emphasize how binding equilibria of catalytic intermediates define the observed enzymatic reactivity. Given the catalytic behavior of HAOr during the spectrophotometric nitrite reduction *in vitro* and the considerably different active site architecture compared with the ancestral ccNiR template, it appears that the HAOr houses an active site that is tuned for NO release.

Indeed, HAOr isolated from the anammox bacterium *K. stuttgartiensis* reduced nitrite to NO when phenazine ethosulfate was used as the electron carrier. The observed low rate of NO production *in vitro* is probably due to suboptimal redox equilibria and the overall disruption of a tightly coupled intracellular multicomponent system, as has been seen before for hydrazine synthesis by HZS (27). Next to the direct measurement of NO production from nitrite reduction with HAOr, and the features of the HAOr active site, the physiology of anammox bacteria strongly suggests that HAOr functions as an NO-producing nitrite reductase *in vivo*. The other reductive catalytic reactions performed by HAOr (reduction of nitrite, hydroxylamine, and NO to ammonium) measured *in vitro* using the much stronger reducing agent methyl viologen cannot be reconciled with anammox catabolism. Under standard growth conditions with limiting nitrite and excess of millimolars of ammonium, the high expression of an ammonia-producing nitrite reductase by anammox bacteria would be unnecessary and energetically inefficient (23). Furthermore, as anammox bacteria use NO to activate ammonium into hydrazine with hydroxylamine as an enzyme-bound intermediate, having a highly abundant enzyme that rapidly reduces both NO and hydroxylamine back to ammonium would be detrimental to hydrazine production, and consequently to cell growth and activity in general as hydrazine synthesis and oxidation are the central pillars of anammox catabolism (25, 27, 31). Indeed, all cellular ammonium oxidation activity stops completely when hydrazine synthesis is blocked by inhibitors or NO scavengers (27). Together with the core catabolic proteins unique to anammox bacteria, hydrazine synthase, and hydrazine dehydrogenase, HAOr is conserved throughout anammox genera including those that lack a conventional nitrite reductase. In addition, when *K. stuttgartiensis* is grown with NO and ammonium, in the absence of nitrite, the transcription of the HAOr complex is strongly downregulated, implicating HAOr in NO production from nitrite *in vivo* (25). Consequently, based on our results and earlier physiological observations, we propose that the first step of the anammox pathway, the reduction of nitrite to NO, is carried out by HAOr.

Evaluating HAOr in the context of the evolution of octaheme oxidoreductases, the close structural and functional relationship between the octaheme HAO protein family and the pentaheme ccNiR stands out. ccNiR has been proposed as the ancestral template from which both OTR and ONR evolved, and the latter led to the emergence of the HAO protein family (11). Both oxidative and reductive HAOs can reduce an array of nitrogen compounds, whereas HAOr is incompetent for oxidative catalysis. This differential functionality within the HAO family, combined with the common ancestor that was a reductase, *i.e.*, ccNiR, suggests that the direct descendant of the ccNiR/ONR branch was a reductive HAO, from which the oxidative HAO homologs emerged. Both structurally and functionally, HAOr represents the core HAO template that functions as a reductase, while oxidative HAOs appear to have acquired an additional catalytic module. This catalytic module enables oxidative catalysis while

simultaneously preventing reductive side-reactivity. Oxidative HAOs appear designed to kinetically favor hydroxylamine oxidation under physiologically relevant conditions even when reduction to ammonia is thermodynamically favorable (16). The oxidative module includes the distinct Tyr-heme cross-link, resulting in a substantially more ruffled P460 cofactor, with a lower midpoint potential compared with the reductive HAOs. Intriguingly, it appears that the information about the direction of catalysis for each HAO homolog is highly conserved on the genomic level, encoded as the absence or presence of the Tyr residue.

Experimental procedures

General considerations

All chemicals used were purchased from Sigma-Aldrich, unless stated otherwise. High-performance liquid chromatography (HPLC)-grade chemicals were purchased from Baker. In total, 18.2 MΩ cm water was used to prepare all buffers and solutions. All protein purification steps took place in ambient air and at 4 °C.

Protein purification

Cells were harvested from a 10-l single-cell continuous membrane bioreactor containing *K. stuttgartiensis* (∼95% pure) (53) and cell lysis proceeded as described previously (54). HAOr was brought to homogeneity in a two-step liquid chromatography procedure using an Äkta Purifier (GE Healthcare). Columns used were packed at a flow rate of 10 ml·min^{-1} (XK 26/20 column, GE Healthcare) and eluted at 5 ml·min^{-1}. The eluate was monitored at 280 nm. Cell-free extract was applied to a column packed with 60 ml of Q Sepharose XL (GE Healthcare) and equilibrated with 20 mM Tris-HCl buffer, pH 8.0. After washing with two column volumes (CV) of 400 mM NaCl in Tris-HCl buffer, pH 8.0, the sample of interest was eluted isocratically with 550 mM NaCl in the same buffer. This fraction was desalted with 20 mM potassium phosphate buffer (KPi), pH 7.0 and concentrated with 100-kDa molecular mass cutoff spin filters (Vivaspin 20; Sartorius Stedim Biotech). The concentrated fraction was loaded onto a 40-ml column packed with Ceramic Hydroxyapatite (Bio-Rad) and equilibrated with 20 mM KPi, pH 7.0. After washing with about 20 CV, HAOr eluted as a near-symmetrical peak during a 30-min linear gradient of 50 to 500 mM KPi, pH 7.0. This peak was collected, desalted as described above, and concentrated to about 150 μM protein. Purity was checked throughout purification by nondenaturating and SDS-denaturing polyacrylamide gel electrophoresis (55). The identity of the protein was established by MALDI-TOF mass spectroscopy (Microflex LT, Bruker Daltonik) on the tryptic digest of SDS-PAGE gel slices of the monomers (56). Enzyme preparations were either used immediately or rapidly frozen in liquid N_2 and stored at −80 °C in aliquots.

UV/Vis spectroscopy and activity assays

UV–visible spectra were recorded at room temperature in quartz cuvettes (Hellma), sealed with rubber stoppers, using a Cary 60 spectrophotometer (Agilent) that was placed inside an anaerobic glove box (N_2/H_2 atmosphere; O_2 <2 ppm). Enzyme assays were carried out in the same glove box at room temperature. All solutions were prepared in serum bottles sealed with rubber stoppers and made anoxic by alternately applying vacuum and Argon for seven times. NO-containing (0.9 mM) stock solution was prepared by sparging anoxic 20 mM KPi, pH 7.0 with an NO-He gas mixture (1:1, v/v) for 10 min. Reaction mixtures (1 ml) in 20 mM KPi, pH 7.0 were prepared in 2-ml quartz cuvettes (path length 10 mm; Hellma Analytics) that were sealed with rubber stoppers. Reactions were initiated by the addition of enzyme (51 nM for the trimeric form of the enzyme: $\alpha_3\beta_3$). Oxidation assays were followed by measuring the reduction of bovine (or equine) cytochrome *c* at 550 nm ($\Delta\varepsilon_{550}$ = 19.6 mM^{-1} cm^{-1}) (57). Reduction assays were followed by measuring the oxidation of either zinc- or dithionite-reduced methyl viologen monocation radical (MVred) at 730 nm (ε_{730} = 2.14 mM^{-1} cm^{-1}) (32). Reaction rates were determined by linear regression fit applied to the first 10% absorbance change and were corrected for background consumption. Values reported are the average of three trials. Michaelis–Menten fits were performed in Origin 2020 (OriginLab Corp).

Membrane-inlet mass spectrometry (MIMS)

Nitric oxide production by HAOr was assayed by measuring the dissolved nitric oxide concentration using MIMS (HPR40, Positive Ion Counting detector, Hiden Analytical). A custom-designed MIMS chamber (58) was used with a final assay volume of 5.7 ml. The MIMS probe was mounted with a 10 μm thin, 8 mm^2 silicon membrane (Hiden Analytical). The electron emission current was set to 100 μA and measurement frequency was set to 1 s^{-1}. Assays were carried out in 20 mM MOPS, 200 mM NaCl, pH 7.5, which was made anaerobic in the MIMS chamber by flushing with Ar at 20 ml min^{-1} at 30 °C. Phenazine ethosulfate (200 μM), ascorbic acid (100 μM) and HAOr (0.7 nM) were added from anaerobic stock solutions. The assay was initiated by the addition of nitrite (50 μM) from an anaerobic stock solution. All additions were made using gastight syringes (Hamilton). The nitric oxide signal was calibrated by adding known amounts of nitric oxide from a stock solution, made by flushing anaerobic MQ water with 4% NO in He for 15 min at 10 ml min^{-1}. Assays were performed in triplicate, and nitric oxide production rates were determined by fitting the initial linear portion of the graph using OriginPro 2020 (OriginLab).

Electrochemical redox titration

Redox titrations of purified HAOr were performed with a home-built optically transparent thin-layer electrochemical cell (OTTLE) that was designed by the workshop of the physical chemistry department of the University of Freiburg as adapted from Baymann *et al.* (59). The OTTLE was connected to a potentiostat (PGSTAT204, Metrohm Autolab) and the spectroscopic changes of the sample upon potentiometric titration were monitored from 400 to 600 nm using a Cary 60 spectrophotometer (Agilent). The Ag/AgCl reference electrode was calibrated against a saturated quinhydrone solution in 1 M

MOPS buffer, pH 7.0 at room temperature (E_m = + 280 mV *versus* SHE (60)). The assay mixture contained 50 μM as isolated HAOr in 50 mM MOPS, pH 7.0, containing 50 mM KCl, 40 mM glucose, 10 U glucose oxidase, 5 U catalase, and a cocktail of mediators (20 μM final concentration for each: ferrocene (E'_0 = +640 mV); ferricyanide (E'_0 = +430 mV); 1.4-benzoquinone (E'_0 = +280 mV); 2,5-dimethyl-1,4-benzoquinone (E'_0 = +180 mV); 1,2-naphthoquinone (E'_0 = +145 mV); phenazine methosulfate (E'_0 = +80 mV); 1,4-naphthoquinone (E'_0 = +60 mV); phenazine ethosulfate (E'_0 = +55 mV); 5-hydroxy-1,4-naphthoquinone (E'_0 = +30 mV); 1,2-dimethyl-1,4-naphthoquinone (E'_0 = 0 mV); 2,5-dihydroxy-p-benzoquinone (E'_0 = −60 mV); 5,8-dihydroxy-1,4-naphthoquinone (E'_0 = −145 mV), 9,10-anthraquinone (E'_0 = −184 mV), 9,10-anthraquinone-2-sulfonate (E'_0 = −225 mV); benzyl viologen (E'_0 = −350 mV); and methyl viologen (E'_0 = −440 mV/−772 mV)).

Titrations were performed from −600 mV to +650 mV (*versus* SHE) at room temperature, in both reductive and oxidative directions, with potential increments of 25 mV. Equilibration time was 10 min per step. HAOr was cycled several times between redox states with no detectable spectral alterations. Spectral changes were evaluated by global fitting of the spectra as a function of potential, using the "mfit-nernst" function in the QSoas software (61) (version 2.1, build 2017.06.27), taking into account six oxidation states (A–F). Using the raw spectra corresponding to each of the six redox states (A–F), the difference spectra corresponding to each of the five transitions were calculated, *e.g.*, the change from state A to state B corresponds to transition 1. The difference spectrum of the total transition (from state A to state F), corresponding to the fully reduced minus fully oxidized states, was also calculated. The mathematical area corresponding to the Soret and the α bands (411–434 nm and 540–570 nm, respectively) was calculated for all discerned transitions (1–5) and for the total transition, using Origin 2020 (OriginLab). Assuming contribution of ten hemes to the total Soret area change and nine to the alpha band, the number of hemes contributing to each redox transition was calculated, based on both the Soret and the α band changes. For each transition, the difference between the heme count from the Soret area and the α band, respectively, corresponded to the single unaccounted heme, *i.e.*, the catalytic heme.

Heme normal coordinate structural decomposition

The heme OOP distortions can be quantitatively assessed by assuming planar porphyrin with D4h symmetry and calculating the distance of specific atoms from this plane. The crystallographic coordinates of each catalytic heme of interest were retrieved from the PDB files and were used as input for the online calculation of heme OOP distortions (41, 43). For NeHAO, chain A, chain C, and chain E were calculated separately, and the average is shown in Figure 1. The same was done for KsHDH, where chain G, chain H, and chain I were used. For KsHAO and HAOr the available monomeric structures were used. The complete output can be found in the Table S1.

Miscellaneous

Ammonia concentration was measured with the colorimetric method described by Taylor *et al.* (62). Nitrite was measured with the Griess reaction as described by Kartal *et al.* (63). Protein concentration was measured with the Bio-Rad protein assay based on the method of Bradford (64), using bovine serum albumin as standard. The identification of the isolated protein complex was confirmed by MALDI-TOF mass spectrometry (56). Each spectrum (900–4000 m/z) was analyzed using the Mascot Peptide Mass Fingerprint (Matrix Science) against the *K. stuttgartiensis* database, allowing methionine oxidation as variable modification, 0.2-Da peptide tolerance, and at most one trypsin miscleavage.

Data availability

Data that are not contained within this article are to be shared upon request.

Supporting information—This article contains supporting information.

Acknowledgments—We thank Jan Keltjens, Frauke Baymann, and Wolfgang Nitschke for insightful discussions, Vincent Fourmond for kindly supplying us with the QSoas software, and Guylaine Nuijten for maintenance of the continuous bacterial cultures.

Author contributions—B. K., C. F., M. S. M. J., and J. R. conceived and designed the research; W. J. M. and C. F. cultivated *Kuenenia stuttgartiensis*; C. F., W. J. M., and R. A. S. purified the protein; C. F. performed UV-vis spectroscopy, activity assays, and out-of-plane heme displacement modeling; C. F., J. R., and S. L. performed electrochemical redox titration; R. A. S. and W. V. performed membrane-inlet mass spectrometry; C. F. performed MALDI-TOF mass spectrometry; C. F. and B. K. wrote the article with input from all the coauthors.

Funding and additional information—C. F. and M. S. M. J. were supported by a Spinoza Prize awarded to M. S. M. J. by the Netherlands Organization for Scientific Research [NWO 62001581, 2012], S. L. and W. V. by [NWO 824.15.011, 2015 awarded to B. K.], W. V. by NWO VI.Vidi.192.001 grant (awarded to Laura van Niftrik) B. K. by the European Research Council [ERC 640422, 2014], and J. R. by [ERC 339880, 2014]. M. S. M. J. was further supported by [ERC 232937, 2009], [ERC 339880, 2014], and [NWO 024002002, 2014].

Conflict of interest—The authors declare no conflicts of interest.

Abbreviations—The abbreviations used are: HAO, hydroxylamine oxidoreductase; MCC, multiheme cytochrome; MIMS, membrane-inlet mass spectrometry; OCC, octaheme cytochrome; ONR, octaheme nitrite reductase; OTR, octaheme tetrathionate reductase; OTTLE, optically transparent thin-layer electrochemical cell; SDS-PAGE, sodium dodecyl sulfate–polyacrylamide gel electrophoresis.

References

1. Richardson, D. J. (2000) Bacterial respiration: A flexible process for a changing environment. *Microbiology* **146**(Pt 3), 551–571

2. Simon, J., Kern, M., Hermann, B., Einsle, O., and Butt, J. N. (2011) Physiological function and catalytic versatility of bacterial multihaem cytochromes *c* involved in nitrogen and sulfur cycling. *Biochem. Soc. Trans.* **39**, 1864–1870
3. Baymann, F., Giusti, F., Picot, D., and Nitschke, W. (2007) The c_i/b_H moiety in the b_6f complex studied by EPR: A pair of strongly interacting hemes. *Proc. Natl. Acad. Sci. U. S. A.* **104**, 519–524
4. Clarke, T. A., Mills, P. C., Poock, S. R., Butt, J. N., Cheesman, M. R., Cole, J. A., Hinton, J. C. D., Hemmings, A. M., Kemp, G., Söderberg, C. A. G., Spiro, S., Van Wonderen, J., and Richardson, D. J. (2008) *Escherichia coli* cytochrome *c* nitrite reductase NrfA. In *Methods in Enzymology*, Elsevier, Amsterdam, the Netherlands: 63–77
5. Edwards, M. J., White, G. F., Butt, J. N., Richardson, D. J., and Clarke, T. A. (2020) The crystal structure of a biological insulated transmembrane molecular wire. *Cell* **181**, 665–673
6. Mowat, C. G., Rothery, E., Miles, C. S., McIver, L., Doherty, M. K., Drewette, K., Taylor, P., Walkinshaw, M. D., Chapman, S. K., and Reid, G. A. (2004) Octaheme tetrathionate reductase is a respiratory enzyme with novel heme ligation. *Nat. Struct. Mol. Biol.* **11**, 1023–1024
7. Atkinson, S. J., Mowat, C. G., Reid, G. A., and Chapman, S. K. (2007) An octaheme *c*-type cytochrome from *Shewanella oneidensis* can reduce nitrite and hydroxylamine. *FEBS Lett.* **581**, 3805–3808
8. Polyakov, K. M., Boyko, K. M., Tikhonova, T. V., Slutsky, A., Antipov, A. N., Zvyagilskaya, R. A., Popov, A. N., Bourenkov, G. P., Lamzin, V. S., and Popov, V. O. (2009) High-resolution structural analysis of a novel octaheme cytochrome *c* nitrite reductase from the haloalkaliphilic bacterium *Thioalkalivibrio nitratireducens*. *J. Mol. Biol.* **389**, 846–862
9. Tikhonova, T. V., Trofimov, A. A., and Popov, V. O. (2012) Octaheme nitrite reductases: Structure and properties. *Biochemistry* **77**, 1129–1138
10. Bergmann, D. J., Hooper, A. B., and Klotz, M. G. (2005) Structure and sequence conservation of hao cluster genes of autotrophic ammonia-oxidizing bacteria: Evidence for their evolutionary history. *Appl. Environ. Microbiol.* **71**, 5371–5382
11. Klotz, M. G., Schmid, M. C., Strous, M., op den Camp, H. J., Jetten, M. S., and Hooper, A. B. (2008) Evolution of an octahaem cytochrome *c* protein family that is key to aerobic and anaerobic ammonia oxidation by bacteria. *Environ. Microbiol.* **10**, 3150–3163
12. Igarashi, N., Moriyama, H., Fujiwara, T., Fukumori, Y., and Tanaka, N. (1997) The 2.8Å structure of hydroxylamine oxidoreductase from a nitrifying chemoautotrophic bacterium, *Nitrosomonas europaea*. *Nat. Struct. Biol.* **4**, 276–284
13. Cedervall, P. E., Hooper, A. B., and Wilmot, C. M. (2009) Crystallization and preliminary X-ray crystallographic analysis of a new crystal form of hydroxylamine oxidoreductase from *Nitrosomonas europaea*. *Acta Crystallogr. Sect. F Struct. Biol. Cryst. Commun.* **65**, 1296–1298
14. Maalcke, W. J., Dietl, A., Marritt, S. J., Butt, J. N., Jetten, M. S., Keltjens, J. T., Barends, T. R., and Kartal, B. (2014) Structural basis of biological NO generation by octaheme oxidoreductases. *J. Biol. Chem.* **289**, 1228–1242
15. Kostera, J., Youngblut, M. D., Slosarczyk, J. M., and Pacheco, A. A. (2008) Kinetic and product distribution analysis of NO• reductase activity in *Nitrosomonas europaea* hydroxylamine oxidoreductase. *J. Biol. Inorg. Chem.* **13**, 1073–1083
16. Kostera, J., McGarry, J., and Pacheco, A. A. (2010) Enzymatic interconversion of ammonia and nitrite: The right tool for the job. *Biochemistry* **49**, 8546–8553
17. Hooper, A. B., and Nason, A. (1965) Characterization of hydroxylamine-cytochrome *c* reductase from the chemoautotrophs *Nitrosomonas europaea* and *Nitrosocystis oceanus*. *J. Biol. Chem.* **240**, 4044–4057
18. Caranto, J. D., and Lancaster, K. M. (2017) Nitric oxide is an obligate bacterial nitrification intermediate produced by hydroxylamine oxidoreductase. *Proc. Natl. Acad. Sci. U. S. A.* **114**, 8217–8222
19. Maalcke, W. J., Reimann, J., de Vries, S., Butt, J. N., Dietl, A., Kip, N., Mersdorf, U., Barends, T. R., Jetten, M. S., Keltjens, J. T., and Kartal, B. (2016) Characterization of anammox hydrazine dehydrogenase, a key N_2-producing enzyme in the global nitrogen cycle. *J. Biol. Chem.* **291**, 17077–17092
20. Akram, M., Dietl, A., Mersdorf, U., Prinz, S., Maalcke, W., Keltjens, J., Ferousi, C., de Almeida, N. M., Reimann, J., Kartal, B., Jetten, M. S. M., Parey, K., and Barends, T. R. M. (2019) A 192-heme electron transfer network in the hydrazine dehydrogenase complex. *Sci. Adv.* **5**, eaav4310
21. Andersson, K. K., Kent, T. A., Lipscomb, J. D., Hooper, A. B., and Münck, E. (1984) Mössbauer, EPR, and optical studies of the P-460 center of hydroxylamine oxidoreductase from *Nitrosomonas*. *J. Biol. Chem.* **259**, 6833–6840
22. Caranto, J. D., Vilbert, A. C., and Lancaster, K. M. (2016) *Nitrosomonas europaea* cytochrome P460 is a direct link between nitrification and nitrous oxide emission. *Proc. Natl. Acad. Sci. U. S. A.* **113**, 14704–14709
23. Kartal, B., de Almeida, N. M., Maalcke, W. J., Op den Camp, H. J., Jetten, M. S., and Keltjens, J. T. (2013) How to make a living from anaerobic ammonium oxidation. *FEMS Microbiol. Rev.* **37**, 428–461
24. Haase, D., Hermann, B., Einsle, O., and Simon, J. (2017) Epsilonproteobacterial hydroxylamine oxidoreductase (εHao): Characterization of a 'missing link' in the multihaem cytochrome *c* family. *Mol. Microbiol.* **105**, 127–138
25. Hu, Z., Wessels, H., van Alen, T., Jetten, M. S. M., and Kartal, B. (2019) Nitric oxide-dependent anaerobic ammonium oxidation. *Nat. Commun.* **10**, 1244
26. Dietl, A., Maalcke, W. J., Ferousi, C., Jetten, M. S. M., Kartal, B., and Barends, T. R. M. (2019) A 60-heme reductase complex from an anammox bacterium shows an extended electron transfer pathway. *Acta Crystallogr. D Struct. Biol.* **75**, 333–341
27. Kartal, B., Maalcke, W. J., de Almeida, N. M., Cirpus, I., Gloerich, J., Geerts, W., Op den Camp, H. J., Harhangi, H. R., Janssen-Megens, E. M., Francoijs, K. J., Stunnenberg, H. G., Keltjens, J. T., Jetten, M. S., and Strous, M. (2011) Molecular mechanism of anaerobic ammonium oxidation. *Nature* **479**, 127–130
28. de Almeida, N. M., Neumann, S., Mesman, R. J., Ferousi, C., Keltjens, J. T., Jetten, M. S., Kartal, B., and van Niftrik, L. (2015) Immunogold localization of key metabolic enzymes in the anammoxosome and on the tubule-like structures of *Kuenenia stuttgartiensis*. *J. Bacteriol.* **197**, 2432–2441
29. van Niftrik, L., Geerts, W. J., van Donselaar, E. G., Humbel, B. M., Yakushevska, A., Verkleij, A. J., Jetten, M. S. M., and Strous, M. (2008) Combined structural and chemical analysis of the anammoxosome: A membrane-bounded intracytoplasmic compartment in anammox bacteria. *J. Struct. Biol.* **161**, 401–410
30. Neumann, S., Wessels, H. J., Rijpstra, W. I., Sinninghe Damste, J. S., Kartal, B., Jetten, M. S., and van Niftrik, L. (2014) Isolation and characterization of a prokaryotic cell organelle from the anammox bacterium *Kuenenia stuttgartiensis*. *Mol. Microbiol.* **94**, 794–802
31. Dietl, A., Ferousi, C., Maalcke, W. J., Menzel, A., de Vries, S., Keltjens, J. T., Jetten, M. S., Kartal, B., and Barends, T. R. (2015) The inner workings of the hydrazine synthase multiprotein complex. *Nature* **527**, 394–397
32. Lawton, T. J., Bowen, K. E., Sayavedra-Soto, L. A., Arp, D. J., and Rosenzweig, A. C. (2013) Characterization of a nitrite reductase involved in nitrifier denitrification. *J. Biol. Chem.* **288**, 25575–25583
33. van Wonderen, J. H., Burlat, B., Richardson, D. J., Cheesman, M. R., and Butt, J. N. (2008) The nitric oxide reductase activity of cytochrome *c* nitrite reductase from *Escherichia coli*. *J. Biol. Chem.* **283**, 9587–9594
34. Suschek, C. V. (2016) Nitric oxide derivatives and skin environmental exposure to light: From molecular pathways to therapeutic opportunities. In: Wondrak, G. T., ed. *Skin Stress Response Pathways: Environmental Factors and Molecular Opportunities*, Springer International Publishing, Cham, Switzerland: 127–154
35. Atwood, J. L., and Lehn, J. M. (1996) *Comprehensive Supramolecular Chemistry: Supramolecular Reactivity and Transport: Bioinorganic Systems*, Pergamon, New York, NY
36. Arciero, D. M., Collins, M. J., Haladjian, J., Bianco, P., and Hooper, A. B. (1991) Resolution of the four hemes of cytochrome *c*554 from *Nitrosomonas europaea* by redox potentiometry and optical spectroscopy. *Biochemistry* **30**, 11459–11465
37. Collins, M. J., Arciero, D. M., and Hooper, A. B. (1993) Optical spectropotentiometric resolution of the hemes of hydroxylamine oxidoreductase. Heme quantitation and pH dependence of Em. *J. Biol. Chem.* **268**, 14655–14662

38. Kleingardner, J. G., and Bren, K. L. (2015) Biological significance and applications of heme *c* proteins and peptides. *Acc. Chem. Res.* **48**, 1845–1852
39. Shelnutt, J. A., Song, X.-Z., Ma, J.-G., Jia, S.-L., Jentzen, W., and Medforth, C. J. (1998) Nonplanar porphyrins and their significance in proteins. *Chem. Soc. Rev.* **27**, 31–42
40. Sun, Y., Benabbas, A., Zeng, W., Kleingardner, J. G., Bren, K. L., and Champion, P. M. (2014) Investigations of heme distortion, low-frequency vibrational excitations, and electron transfer in cytochrome *c*. *Proc. Natl. Acad. Sci. U. S. A.* **111**, 6570
41. Liptak, M. D., Wen, X., and Bren, K. L. (2010) NMR and DFT investigation of heme ruffling: Functional implications for cytochrome *c*. *J. Am. Chem. Soc.* **132**, 9753–9763
42. Graves, A. B., Graves, M. T., and Liptak, M. D. (2016) Measurement of heme ruffling changes in MhuD using UV–vis spectroscopy. *J. Phys. Chem. B* **120**, 3853
43. Jentzen, W., Song, X.-Z., and Shelnutt, J. A. (1997) Structural characterization of synthetic and protein-bound porphyrins in terms of the lowest-frequency normal coordinates of the macrocycle. *J. Phys. Chem. B* **101**, 1684–1699
44. Ding, X. D., Weichsel, A., Andersen, J. F., Shokhireva, T. K., Balfour, C., Pierik, A. J., Averill, B. A., Montfort, W. R., and Walker, F. A. (1999) Nitric oxide binding to the ferri- and ferroheme states of nitrophorin 1, a reversible NO-binding heme protein from the saliva of the blood-sucking insect, *Rhodnius prolixus*. *J. Am. Chem. Soc.* **121**, 128–138
45. Andersen, J. F., Ding, X. D., Balfour, C., Shokhireva, T. K., Champagne, D. E., Walker, F. A., and Montfort, W. R. (2000) Kinetics and equilibria in ligand binding by nitrophorins 1–4: Evidence for stabilization of a nitric oxide–ferriheme complex through a ligand-induced conformational trap. *Biochemistry* **39**, 10118–10131
46. Ford, P. C., Fernandez, B. O., and Lim, M. D. (2005) Mechanisms of reductive nitrosylation in iron and copper models relevant to biological systems. *Chem. Rev.* **105**, 2439–2456
47. Rinaldo, S., Arcovito, A., Brunori, M., and Cutruzzolà, F. (2007) Fast dissociation of nitric oxide from ferrous *Pseudomonas aeruginosa* cd_1 nitrite reductase: A novel outlook on the catalytic mechanism. *J. Biol. Chem.* **282**, 14761–14767
48. Radoul, M., Bykov, D., Rinaldo, S., Cutruzzola, F., Neese, F., and Goldfarb, D. (2011) Dynamic hydrogen-bonding network in the distal pocket of the nitrosyl complex of *Pseudomonas aeruginosa* cd_1 nitrite reductase. *J. Am. Chem. Soc.* **133**, 3043–3055
49. Einsle, O., Messerschmidt, A., Stach, P., Bourenkov, G. P., Bartunik, H. D., Huber, R., and Kroneck, P. M. (1999) Structure of cytochrome *c* nitrite reductase. *Nature* **400**, 476–480
50. Judd, E. T., Stein, N., Pacheco, A. A., and Elliott, S. J. (2014) Hydrogen bonding networks tune proton-coupled redox steps during the enzymatic six-electron conversion of nitrite to ammonia. *Biochemistry* **53**, 5638–5646
51. Bykov, D., and Neese, F. (2015) Six-electron reduction of nitrite to ammonia by cytochrome *c* nitrite reductase: Insights from density functional theory studies. *Inorg. Chem.* **54**, 9303–9316
52. Lukat, P., Rudolf, M., Stach, P., Messerschmidt, A., Kroneck, P. M., Simon, J., and Einsle, O. (2008) Binding and reduction of sulfite by cytochrome *c* nitrite reductase. *Biochemistry* **47**, 2080–2086
53. Kartal, B., van Niftrik, L., Keltjens, J. T., Op den Camp, H. J., and Jetten, M. S. (2012) Anammox—growth physiology, cell biology, and metabolism. *Adv. Microb. Physiol.* **60**, 211–262
54. Ferousi, C., Lindhoud, S., Baymann, F., Hester, E. R., Reimann, J., and Kartal, B. (2019) Discovery of a functional, contracted heme-binding motif within a multiheme cytochrome. *J. Biol. Chem.* **294**, 16953–16965
55. Laemmli, U. K. (1970) Cleavage of structural proteins during the assembly of the head of bacteriophage T4. *Nature* **227**, 680–685
56. Farhoud, M. H., Wessels, H. J. C. T., Steenbakkers, P. J. M., Mattijssen, S., Wevers, R. A., Van Engelen, B. G., Jetten, M. S. M., Smeitink, J. A., Van Den Heuvel, L. P., and Keltjens, J. T. (2005) Protein complexes in the archaeon *Methanothermobacter thermautotrophicus* analyzed by blue native/SDS-PAGE and mass spectrometry. *Mol. Cell. Proteomics* **4**, 1653–1663
57. Guo, M., Bhaskar, B., Li, H., Barrows, T. P., and Poulos, T. L. (2004) Crystal structure and characterization of a cytochrome *c* peroxidase-cytochrome *c* site-specific cross-link. *Proc. Natl. Acad. Sci. U. S. A.* **101**, 5940–5945
58. Schmitz, R. A., Pol, A., Mohammadi, S. S., Hogendoorn, C., van Gelder, A. H., Jetten, M. S. M., Daumann, L. J., and Op den Camp, H. J. M. (2020) The thermoacidophilic methanotroph *Methylacidiphilum fumariolicum* SolV oxidizes subatmospheric H_2 with a high-affinity, membrane-associated [NiFe] hydrogenase. *ISME J.* **14**, 1223–1232
59. Baymann, F., Moss, D. A., and Mäntele, W. (1991) An electrochemical assay for the characterization of redox proteins from biological electron transfer chains. *Anal. Biochem.* **199**, 269–274
60. Moffet, D. A., Foley, J., and Hecht, M. H. (2003) Midpoint reduction potentials and heme binding stoichiometries of de novo proteins from designed combinatorial libraries. *Biophys. Chem.* **105**, 231–239
61. Fourmond, V. (2016) QSoas: A versatile software for data analysis. *Anal. Chem.* **88**, 5050–5052
62. Taylor, S., Ninjoor, V., Dowd, D. M., and Tappel, A. L. (1974) Cathepsin B_2 measurement by sensitive fluorometric ammonia analysis. *Anal. Biochem.* **60**, 153–162
63. Kartal, B., Koleva, M., Arsov, R., van der Star, W., Jetten, M. S., and Strous, M. (2006) Adaptation of a freshwater anammox population to high salinity wastewater. *J. Biotechnol.* **126**, 546–553
64. Bradford, M. M. (1976) A rapid and sensitive method for the quantitation of microgram quantities of protein utilizing the principle of protein-dye binding. *Anal. Biochem.* **72**, 248–254